

1 **Factors influencing chloride deposition in a coastal hilly area and application to**
2 **chloride deposition mapping**

3
4 Huade Guan^{1,2}, Andrew J. Love^{1,3}, Craig T. Simmons^{1,2}, Ahmet S. Kayaalp⁴, Oleg Makhnin⁵

5
6 1. School of Chemistry, Physics and Earth Sciences, Flinders University, Australia

7
8 2. National Centre for Groundwater Research and Training, Australia

9
10 3. Department of Land, Water, and Biodiversity Conservation, South Australia

11
12 4. Water Technology Division, Water Corporation, West Australia

13
14 5. Department of Mathematics, New Mexico Institute of Mining and Technology, U.S.A.

15
16
17
18 Contact:

19 Dr. Huade Guan, School of Chemistry, Physics & Earth Sciences, Flinders University,
20 Australia, +61 8 82012319, huade.guan@flinders.edu.au

21
22

23 Abstract

24 Chloride is commonly used as an environmental tracer for studying water flow and
25 solute transport in the environment. It is especially useful for estimating groundwater
26 recharge based on the commonly used chloride mass balance (CMB) method. Strong spatial
27 variability in chloride deposition in coastal areas is one difficulty encountered in
28 appropriately applying the method. A high resolution chloride deposition map in the coastal
29 region is thus needed. The aim of this study is to construct chloride deposition map in the
30 Mount Lofty Ranges (MLR), a coastal hilly area of approximately 9000 km² spatial extent in
31 South Australia. We examined geographic, orographic, and atmospheric factors influencing
32 chloride deposition, using partial correlation and regression analyses. The results indicate
33 that coastal distance, and terrain aspect and slope are two most significant factors controlling
34 chloride deposition in the study area. Coastal distance accounts for 65% spatial variability in
35 chloride deposition, with terrain aspect and slope for 8%. The average deposition gradient is
36 about 0.08 gm⁻²year⁻¹km⁻¹ as one progresses inland. The results are incorporated into a
37 published de-trended residual kriging approach (ASOADEK) to produce a 1 km × 1 km
38 resolution bulk chloride deposition and concentration maps. The average uncertainty of the
39 deposition map is about 20% in the western MLR, and over 50% in the eastern MLR. The
40 maps will form a very useful basis for examining catchment chloride balances for use in the
41 CMB application in the study area.

42

43 Key words

44 Chloride deposition, orographic effect, chloride mass balance, kriging, multivariate
45 regression, partial correlation

46

47 1. Introduction

48
49 Chloride is commonly used as an environmental tracer for studying water flow and
50 solute transport in surface water bodies (Dunn and Bacon, 2008; Shaw et al., 2008;
51 Hrachowitz et al., 2009), vadose zones and aquifers (Eriksson and Khunakasem, 1969;
52 Walker et al., 1991; Cook et al., 1992; Phillips, 1994; Wood and Sanford, 1995; Kirchner et
53 al., 2000; Edmunds et al., 2002; Scanlon et al., 2002; Minor et al., 2007). It is especially
54 useful to estimate groundwater recharge based on chloride mass balance (CMB). The CMB
55 method can be applied either for estimating point recharge with chloride concentration in the
56 steady-state soil profile, or for estimating catchment-average recharge with chloride
57 concentration in mean groundwater. For situations that the atmospheric input is the only
58 chloride source, and that no chloride sinks exist in the system, the CMB method can be
59 formulated as

60

$$61 \quad C_p P = C_g G + C_r R \quad (1)$$

62

63 where C_p is chloride concentration in bulk precipitation, P is average precipitation, C_g is
64 chloride concentration in the soil water far below the root zone or in groundwater that was
65 recharged from the catchment, G is groundwater or soil water that is equilibrium with the
66 surface conditions, C_r is chloride concentration in the runoff R . The CMB method does not
67 require knowledge of dynamic hydrological processes (although with such information, it
68 would help to apply the CMB method more reliably). Thus, the method provides a good
69 solution to estimate catchment groundwater recharge in mountainous terrains where
70 hydrogeological and hydrometeorological conditions are complex (Wilson and Guan, 2004).
71 In order to apply the CMB method, the atmospheric chloride input must be known. In the
72 inland area, atmospheric chloride deposition does not change much over a large distance (e.g.,
73 ~100 km) (Keywood et al., 1997). One estimate of average chloride deposition either directly
74 from bulk precipitation sampling, or inferred from the ratio of $^{36}\text{Cl}/\text{Cl}$ which has a 30%
75 uncertainty (Scanlon, 2000), is often used in the CMB calculation. In the coastal area,
76 however, large spatial variability of chloride deposition is often observed (Blackburn and
77 McLeod, 1983; Keywood et al., 1997; Kayaalp, 2001; Biggs, 2006; Alcalá and Custodio,
78 2008a). A detailed map of atmospheric chloride deposition is thus needed to apply the CMB
79 approach for estimating groundwater recharge in the coastal areas.

80 It is commonly accepted that the primary source of the atmospheric chloride is from
81 the ocean by wind-induced whitecaps and bursts, which inject sea water drops into the
82 atmosphere (Lewis and Schwartz, 2004). About 10% of total chloride in the sea salt aerosols
83 moves into the continents, and the majority of this chloride is deposited within 100 km of the
84 coastal area (Eriksson, 1959; Eriksson, 1960). It should be noted that the anthropogenic
85 sources may add chloride to the atmosphere at some extreme situations where air pollution is
86 serious (Alcala and Custodio, 2008b). Two primary mechanisms, dry deposition and wet
87 deposition, control chloride removal from the atmosphere to the land surface. Chloride-
88 bearing aerosols can settle down to the surface by gravitational forces. This dry deposition
89 process is highly dependent on wind conditions and the aerosol size. Chloride in the aerosols
90 can also be rained out from the cloud, or washed out by the falling rain drops. This wet
91 deposition process is dependent on precipitation characteristics. In terms of hydrological
92 applications, it is the total chloride deposition (bulk chloride deposition, or BCD hereafter),
93 i.e., the sum of wet and dry depositions, that is important because it gives the input chloride
94 for the CMB calculation (Wood and Sanford, 1995). Thus, BCD is usually measured from
95 accumulated rain samples over a certain period, with samplers sitting in an open area, and
96 open to the sky all the time. As chloride-bearing aerosols originate from the ocean, it is
97 typically observed that BCD over the continents decays exponentially with increasing
98 distance from the coast (coastal distance hereafter) (Keywood et al., 1997; Gustafsson and
99 Larsson, 2000). Over a short distance, linear relationship can be used to approximate the
100 change of BCD with coastal distance (Alcala and Custodio, 2008a). The relationship between
101 elevation and BCD has been implicitly shown, but not conclusive remark is made as the other
102 effect such as coastal distance was not separated (Contreras et al., 2008).

103 This coastal distance dependence, when quantitatively determined, is useful to
104 estimate BCD for a point location at some known distance from the coast. However, two
105 difficulties exist to directly apply coastal distance dependent relationship in chloride
106 deposition mapping. First, due to coastal distance dependence is physically resulted from how
107 efficiently the atmospheric chloride is moved inland, and how quickly it falls out or is
108 precipitated out, the function parameterization is different from places to places (Alcala et al.,
109 2008a). Second, it is difficult to determine coastal distance because this distance should be
110 calculated from the coastal point that is upwind from the mapping pixel. However, deposition
111 processes are also associated with the prevailing wind direction and it is therefore difficult to
112 use the distance dependence function alone to construct good resolution BCD maps.
113 Instead Thus, kriging is frequently used to map BCD. Carratala et al. (1998) performed

114 ordinary kriging with 28 data points to construct 10 km × 15 km resolution bulk chloride
115 concentration map on the eastern coast of Spain. Gustafsson and Larsson (2000) applied
116 ordinary block kriging to construct 10 km × 10 km resolution seasonal BCD maps with 49
117 data points over an area of 8×10^4 km² in southern Sweden. Alcala and Custodio (2008a) used
118 ordinary kriging to produce 10 km × 10 km mean annual BCD map with measurements over
119 200 geographic points for continental Spain (5×10^5 km²). The ratio of data points over
120 mapping pixels of the above three mapping exercises ranges from one 16th to about one 60th.
121 In the coastal area, BCD often varies significantly even over a few kilometres (Kayaalp,
122 2001). The aim of this study is to construct BCD map at a spatial resolution of 1 km × 1 km
123 over an area of 9000 km², based on 17 data points. In contrast to earlier mapping studies, the
124 ratio of data points over mapping pixels in this study is only one 500th. The sparse data points
125 and small sample size largely increase uncertainty of the kriging estimates (Chang et al.,
126 1998).

127 Can we incorporate some associated physical process information, including coastal
128 distance dependence, so as to make more reliable estimates for chloride deposition to form a
129 basis for BCD mapping? In this context, geostatistical approaches, such as residual kriging
130 (RK), kriging with external drift (KED), and cokriging (CK), can be used to incorporate
131 secondary variable information in the mapping (Isaaks and Srivastava, 1989; Goovaerts, 2000;
132 Guan et al., 2005). Because of the difficulty to select appropriate secondary variables and
133 functions, RK is chosen, in which the secondary variable effect, often called trend estimate, is
134 determined first (Isaaks and Srivastava, 1989, p532). Similar approach has been successfully
135 applied in precipitation and rain water isotope mapping in mountainous terrains (Guan et al.,
136 2005; Guan et al., 2009). The objectives of this study are first to examine the influencing
137 factors associated with physical processes that control chloride deposition by correlation and
138 regression analyses, and based on this to construct BCD map by RK. To do this, we first
139 need to overcome the two previously mentioned difficulties in incorporating coastal distance
140 in the mapping. For the first difficulty, over a small area where the wind and precipitation
141 climate is relatively simple, it is likely that one parameterization of coastal dependence
142 function can be applied. In terms of second difficulty, for simple coastal line geometry, the
143 pixel geographical coordinates may be used as an approximate for coastal distance. Such
144 simplification will be used in this study, with details described in the methodology section
145 (correlation analysis).

146 The study is based on Adelaide and the Mount Lofty Ranges (MLR) of South
147 Australia. The whole area has 1.2 million residents, with 60% water supply coming from on

148 the MLR. A reliable BCD map is important for water resources management over the region.
149 To understand the influencing factors on BCD in the study area, our starting hypotheses are
150 that in addition to coastal distance, (1) windward slopes, associated with sea breeze and in-
151 coming moisture direction, enhance BCD due to topographic interception, and orographic
152 precipitation, and (2) elevation enhances BCD due to increasing precipitation. Although
153 vegetation canopy may influence BCD (Moreno et al., 2001), as bulk chloride samples used
154 in this study were collected in the open area, the canopy effect is not accessed. (This may
155 result in a BCD map deviated from (more likely smaller than) the actual BCD over the area
156 because the difference in BCD over the canopy area and open area is not considered). The
157 results indicate that terrain slope and aspect (slope orientation), associated with prevailing
158 wind direction, may influence BCD in the coastal area, but in a manner that is contrary to our
159 starting hypothesis. The elevation does not significantly affect BCD. These results are
160 helpful to improve our understanding of sea salt deposition in the coastal area. ~~These new~~
161 findings are incorporated into BCD mapping for the study area. The mapping result is
162 compared to ordinary kriging estimates, and cross validated with the observation data. The
163 chloride map produced here will be used to examine the catchment chloride balance status,
164 which is to be discussed in a subsequent paper.

165 **2. Methodology**

166 **2.1 Study area and data**

167 The study area lies in and to the east of Adelaide, South Australia (Fig. 1). It covers
168 an area of about 9000 km², with topographic relief of 700 m. To the west is Gulf St-Vincent,
169 which extends about 150 km long and 70 km wide. To the south is the Southern Ocean, with
170 saline lake Alexandria sitting to the southwest. The primary industries include health service,
171 education, winery and agriculture. No obvious air pollution sources of chlorine exist in the
172 area. The bedrock in the MLR is primarily late Precambrian metamorphous sedimentary rock
173 composed of shale and sandstone, and some limestone (Preiss, 1987). The climate is of
174 Mediterranean type, with wet winters and dry summers. The annual precipitation ranges from
175 below 300 mm to above 1000 mm, with an areal average of 600 mm (Guan et al., 2009).
176 Mean daily temperature over the area is about 15-18°C. The annual pan evaporation at a
177 location of 600-mm precipitation (about area-average value) is about 1500 mm (BOM, 2009).
178 Prevailing westerly moisture flux feeds precipitation (Guan et al., 2009), and thus wet
179 chloride deposition in the area. In term of dry chloride deposition, Gulf St Vincent to the west,

180 and Southern Ocean to the south can provide marine aerosols to the study area. These two
181 marine chloride sources can be brought into the study area by westerly winds and southerly
182 winds, respectively. Westerly sea breezes occur frequently during part of the day (Fig. 2, and
183 later Fig. 9) over most of the study area, which fuel atmospheric transport of sea salt aerosols
184 from ~~the~~ Gulf St Vincent and facilitate dry deposition. In contrast, the southerly wind is not
185 dominant in the study area, even at ~~At the south edge of the area(Fig. 2), no dominant~~
186 ~~southerly wind is observed.~~ Thus, from both wet and dry deposition points of view, dominant
187 atmospheric chloride source in this area is from the west, i.e., from Gulf St Vincent by wind,
188 and from larger distance in atmospheric moisture for precipitation over the area. Southern
189 Ocean may provide some additional atmospheric chloride source, but its effect is secondary. -

190 Bulk chloride concentration was measured at 17 sites in the open area, over two
191 periods by two organizations: Flinders University (1992-1994) and Department of Water,
192 Land and Biodiversity Conservation (DWLBC) (2002-2005) (Table 1). It is BCD in the open
193 area that is examined in this study. Although canopy may change chloride deposition rates, its
194 effect is difficult to evaluate because this information is not included in our samples.
195 DWLBC samples were multiple-month cumulative rain, while Flinders samples were
196 collected daily and summed to monthly. For DWLBC sampling, following common
197 procedure (Friedman et al., 1992), a thin layer of mineral oil was applied in the collectors to
198 avoid water evaporation over the two sampling periods (although evaporation is not critical in
199 measuring BCD). On average the sampling duration is about 2 years, with two sites (Sites 4
200 and 5) sampled for shorter than one year. They are nevertheless included because the
201 sampling period covers both halves of the dry and rainy seasons. Both rain sample volume
202 and chloride concentration were measured for each cumulative sample. Chloride
203 concentration was measured with an ion chromatography system, with standard deviation of
204 repeat testings less than 0.1 mg/l over the normal sample concentration range, at Land and
205 Water Division of the Commonwealth Scientific and Industrial Research Organization,
206 Adelaide, Australia. Average chloride concentrations and annual chloride deposition are
207 calculated from samples at each of the 17 sites (Table 1). In addition, wind direction data for
208 41 sites in and near the study area were obtained from the Bureau of Meteorology of
209 Australia (BOM) (Fig. 1). Wind direction was recorded twice daily at 9:00AM and 3:00PM
210 local time.

211 **2.2 Correlation analysis**

212 Correlation analysis has been widely used to examine linear association between
 213 variables. The Pearson product-moment correlation coefficient (r) is the most common
 214 measure of linear association between two variables. When multiple variables are correlated
 215 to one another, the correlation coefficient of the variable of interest with any one of the other
 216 variables may give association implication which is not physically dependent. To solve this
 217 problem, a partial correlation coefficient is applied to examine the linear correlation between
 218 the two variables with the effects of other selected variables removed (Lowry, 1999-2009).
 219 An example of partial correlation coefficient between variables x and y independent of a third
 220 variable (z) is calculated using

$$221 \quad r_{xy(z)} = \frac{r_{xy} - r_{xz}r_{yz}}{\sqrt{1 - r_{xz}^2} \sqrt{1 - r_{yz}^2}} \quad (2)$$

222 where r is Pearson correlation coefficient between the two variables denoted in the subscripts.
 223 The partial correlation coefficients are calculated with MATLAB in this study. After $r_{xy(z)}$ is
 224 obtained, the significance is tested with a t -distribution. The t -value is calculated by

$$225 \quad t = \frac{r_{xy(z)}}{\sqrt{(1 - r^2)/(N - 2)}} \quad (3)$$

226 where N (≥ 6) is the number of samples (Lowry, 1999-2009). Strictly speaking, the
 227 significance testing relies on the assumption that each variable is spatially independent,
 228 which is often invalid for regionalized random variables, such as the ones examined here.
 229 Thus, the p -values from the correlation analysis are not strictly correct. Nevertheless, they
 230 should be still useful to compare which variables are more important than others to be
 231 associated with **bulk** chloride deposition, and to determine which variables are not significant
 232 (details are discussed in the Results section). This loose significance test is applied to
 233 examine our two hypotheses, one relating to the elevation effect and the other **relating**
 234 **to associated with** -terrain aspect (slope orientation) effect on BCD. If the tested factor is
 235 important in BCD, the partial correlation coefficient between BCD and the factor variable
 236 should have a corresponding p values much smaller than others.

237 It is easy to quantify elevation, terrain aspect and slope for each sampling points. For
 238 coastal distance, we use geographic coordinate X (e.g. Universal Transverse Mercator, or

239 UTM easting) for the chloride aerosol with a source from Gulf St Vincent, and -Y (UTM
 240 northing) for the chloride aerosol with a source from Southern Ocean. Given the relative
 241 position of the study area and the two likely marine aerosol sources, this approximation is
 242 acceptable.

243 **2.3 ASOAdEK regression and mapping**

244 A multivariate regression embedded in a geostatistical model (Auto-searched
 245 Orographic and Atmospheric effects De-trended Kriging, or ASOAdEK) has been shown to
 246 successfully capture geographic and orographic effects on precipitation distribution over
 247 mountain terrains (Guan et al., 2005). The ASOAdEK model has two components: a
 248 regression to obtain the trend estimates, and a residual kriging to compensate where the
 249 regression estimate is poor. The regression was originally developed to auto-search the
 250 effects of atmospheric moisture gradient, prevailing moisture flux direction associated terrain
 251 aspect and slope, and terrain elevation, on precipitation distribution. Recently, it was applied
 252 to examine orographic effects on rain isotope distribution (Guan et al., 2009). Since wet
 253 deposition occurs with precipitation, and dry deposition over the area has similar dominant
 254 westerly source (supported by correlation analysis later) as precipitation, we attempt to use
 255 the ASOAdEK regression to examine the effects of selected geographic and topographic
 256 variables on BCD. The original regression model, including both elevation and terrain aspect,
 257 can be found in (Guan et al., 2005). The regression model used below including elevation,
 258 terrain aspect and slope, first appears in (Guan et al., 2009).

$$259 \quad D = b_0 + b_1X + b_2Y + b_3Z + b_4\beta \cos \alpha + b_5\beta \sin \alpha \quad (4)$$

260 where D is annual BCD (gm^{-2}), X and Y are geographic coordinates (usually as easting and
 261 northing in ~~the Universal Transverse Mercator (UTM)~~ UTM -coordinate system, in km), used
 262 to capture the effect of coastal distance dependence, Z is above-sea-level terrain elevation in
 263 kilometres, β is the slope angle in degree, α is the terrain aspect, defined as the direction of
 264 slope orientation, zero to the north, increasing clockwise, and 180 to the south. The two
 265 trigonometric terms are derived from $\cos(\alpha - \omega)$, where ω is the source flux direction. This
 266 function has a value of 1 at windward slopes, and -1 at leeward slopes. This formulation was
 267 originally designed to capture the orographic effect of more precipitation (or chloride
 268 deposition) on the windward slope than on the leeward side. If chloride deposition is
 269 enhanced in the leeward side, the sign of b_4 and b_5 will be reversed. For situations where the

270 sample size is small, only the terms of statistical significance should be included in the
 271 regression. As discussed later, only two predictor variables are applied for BCD distribution
 272 in the study area.

273 After regression is performed, it is used to generate a regression estimate map (the
 274 trend) based on a DEM. The difference between the observations and regression estimates are
 275 then used to generate a de-trended residual map by ordinary kriging. The final BCD map is
 276 the sum of the regression map and the residual map. This procedure is simply called
 277 ASOAdEK mapping. More details of this approach can be found in (Guan et al., 2005). The
 278 performance of this mapping approach is examined by cross validation, in which each of the
 279 total N data points is set aside each time to compare with the mapping estimate at the location
 280 based on the remaining (N-1) data points (Isaaks and Srivastava, 1989). Both regression and
 281 semivariogram modeling are performed for each cross validation set. The mapping result is
 282 also compared to direct ordinary kriging of the observed chloride depositions. This is called
 283 direct kriging, to be distinguished from the residual kriging, which is one component of the
 284 ASOAdEK model. All kriging calculations are performed with Geostatistical Software
 285 Library (Deutsch and Journel, 1998). Finally, the bulk chloride concentration map is then
 286 constructed based on the annual chloride deposition map and annual precipitation map of the
 287 study area, both at a spatial resolution of 1 km × 1 km.

288 After the ASOAdEK mapping, the uncertainty originated from the mapping approach
 289 is calculated. The mapping uncertainty (ε) is composed of the regression uncertainty and
 290 residual kriging uncertainty. With an assumption that the mapping uncertainty follows normal
 291 distribution, it is calculated as

$$292 \quad \varepsilon = u\sqrt{\varepsilon_r^2 + V_k} \quad (5)$$

293 where u is the critical value of the standard normal distribution, (1.645 for 90%, and 1.960 for
 294 95% confidence level), ε_r is the standard error of the regression fit, and V_k is kriging variance.
 295 A confidence level of 90% is used in this study.

296 **3. Results**

297 **3.1 Correlation analysis and hypothesis testing**

298 As discussed in 2.1, dominant marine chloride source to the study area -both wet and
 299 dry deposition in the study area tend to tend to come from a westerly direction. Chloride

300 deposition data of most ~~of the 17~~ sites (Table 1, Fig. 3) follows this trend except for sites 16
301 and 17. However, at sites 16 and 17, chloride deposition is abnormally high in comparison to
302 site 15. This is probably because Southern Ocean source chloride aerosol becomes important
303 at these two sites. Thus, sites 16 and 17 are excluded from correlation and regression
304 analysis, to avoid their ~~anomalous~~ disturbance on investigating the physical processes of
305 BCD from the primary marine source common to the whole area. However, sites 16 and 17
306 are included for residual kriging and to generate the chloride deposition map. Although an
307 exponential decrease in bulk chloride deposition (D) with increasing coastal distance
308 (approximately X and Y corresponding to two possible marine chloride aerosol sources in
309 the study area) is reported at a large scale (Keywood et al., 1997; Gustafsson and Larsson,
310 2000), a linear relationship is observed between D and X in the study area with coastal
311 distance within 100 km (Fig. 3). This feature supports that a linear correlation and regression
312 analyses between D and X is appropriate over the spatial scale of the study area.

313 With sites 16 and 17 excluded, the correlation matrix of chloride deposition with
314 precipitation and five selected variables is included in Table 2. Based on a one-tailed t test,
315 $|r|$ needs to be 0.44 for a significant level of $p = 0.05$, and 0.35 for $p = 0.10$ given a sample
316 size of 15 (Lowry, 1999-2009). Because of spatial dependence of the examined variables, the
317 significant threshold $|r|$ should be larger than the above values at each confidence level, but
318 the exact line is difficult to define. Nevertheless, these values are useful to determine which
319 variables are not significantly associated with D . For example, based on the r values, Z
320 and $\beta \cos \alpha$ are not significantly correlated to D . The r and p values should be also useful to
321 evaluate relative significance of linear association between D and each of the other examined
322 variables. D and X (easting) have the highest negative correlation. This is consistent with the
323 dominant westerly chloride source for the study area and coastal distance-dependent chloride
324 deposition reported in the literature. ~~The r values suggest that P (precipitation) is correlated~~
325 ~~with D , but also with X . As P (precipitation), Y (northing) and $\beta \sin \alpha$ are both all~~ correlated
326 with X . Based on the correlation matrix, it is difficult to evaluate the association of each of
327 the P , Y , and $\beta \sin \alpha$ with D . Partial correlation coefficients (Fig. 4), with the effect of X
328 removed, suggest that Y and P are not significantly associated with D . That D is not
329 dependent of Y supports that the Southern Ocean marine aerosol source is not important for
330 BCD in the study area. -The relative significance test indicates that $\beta \sin \alpha$ is the second
331 significant term, next to X , correlated with D . This implies that slope and aspect may affect

332 BCD. With X and P effect removed, the correlation between D and $\beta \sin \alpha$ is similar to that
333 with X effect removed, ~~suggesting that dry deposition may be affected by terrain aspect and~~
334 ~~slope. With precipitation effect removed, partial correlation coefficient between D and X is~~
335 ~~0.76, suggesting that dry deposition has a similar coastal distance dependence as BCD.~~
336 Partial correlation analysis results confirm the insignificant association between D and Z , and
337 between D and $\beta \cos \alpha$.

338 We now examine the two hypotheses, (1) elevation and (2) west-facing slope
339 facilitating chloride deposition, as they pertain to possible topographic influences on chloride
340 deposition. Elevation apparently does not enhance chloride deposition, as no significant
341 linear association is found from either the correlation matrix or the partial correlation analysis.
342 Terrain aspect and slope are the second significant factor, next to the coastal distance, for
343 BCD in the study area, as indicated by the partial correlation between D and $\beta \sin \alpha$. The
344 partial correlation coefficient between the two variables is positive. Based on the definition of
345 terrain aspect α in Eq. (4), it has a positive value on east-facing slopes. This indicates that
346 more chloride deposition occurs on eastern slopes (leeward slopes) in respect to the primary
347 atmospheric chloride source direction, instead of on the western (windward) slopes in our
348 starting hypothesis.

349 **3.2 Regression analysis and ASOAdEK mapping**

350 Based on partial correlation analysis, among the five predictor variables in Eq. (4), the
351 two most significantly linearly associated factors to BCD are X and $\beta \sin \alpha$. Thus, regression
352 is performed with X and $\beta \sin \alpha$ only (Table 3). The results indicate that coastal distance
353 explains about 65% of the spatial variability in westerly-source chloride deposition in the
354 study area, while terrain aspect accounts for an additional 8%. Based on the regression results,
355 the chloride deposition gradient average over the study area is about $0.08 \text{ gm}^{-2}\text{year}^{-1}\text{km}^{-1}$
356 downwind away from the coast of Gulf St Vincent. This value is within the range of 0.05 to
357 $0.25 \text{ gm}^{-2}\text{year}^{-1}\text{km}^{-1}$ reported for Spain's non-polluted Mediterranean coastal areas (Alcala
358 and Custodio, 2008a).

359 After regression is performed, it can be used to construct the BCD regression map and
360 ASOAdEK map. To examine the mapping performance, cross validation was performed in
361 comparison to the direct ordinary kriging. One example of cross-validation semivariogram
362 model for direct kriging is shown in Fig. 5a. It is similar among 17 sets of cross-validation

363 data. The semivariogram models for cross-validation residual sets are not shown, as they are
364 different among the 15 sets. In comparison to direct kriging, both regression and ASOADeK
365 estimates give a smaller mean absolute error (MAE), calculated from all cross-validation sets,
366 and higher correlation coefficient between the estimates and observations (Fig. 6a). The MAE
367 value of regression cross validation is 0.80 g/m^2 , about 20% of average observation values
368 over the first 15 locations in Table 1, and the MAE value of ASOADeK cross validation is
369 0.84 g/m^2 , about 21% of the observation average. ASOADeK cross validation results slightly
370 degrades in comparison to that of the regression, probably because the chloride network
371 density is too low. The residual kriging is nevertheless applied because sites 16 and 17 were
372 not included in the regression.

373 Comparison of cross validations provides us confidence to construct BCD map using
374 the ASOADeK ~~model~~ method. The various maps derived from ASOADeK mapping approach
375 are included in Fig. 7a-d. The regression map (Fig. 7a, Table 1) primarily shows the coastal
376 distance and terrain aspect and slope effects. It underestimates chloride deposition in the
377 southeastern corner of the area, because the two data points (16 and 17 in Table 1, probably
378 influenced by the secondary marine aerosol source) were not included in the regression,
379 which was aimed to estimate BCD distribution resulted from the primary westerly marine
380 aerosol source. The residual kriging is performed with the semivariogram model shown in
381 Fig. 5b. The regression underestimates in the southeastern corner are compensated by large
382 positive residuals (Fig. 7b). The chloride deposition map (Fig. 7c) is constructed as the sum
383 of regression and residual maps. Overall, annual chloride deposition rate is over 6 gm^{-2} in the
384 southwestern corner and western coast, decreasing to $4\text{-}5 \text{ gm}^{-2}$ in the central part, and to
385 below 2 gm^{-2} in the eastern and northeastern edges of the area. The mapping uncertainty is
386 calculated based on Eq. (5) and shown in Figure 7d, with BCD observation sites included for
387 comparison. The average uncertainty in the western half is some 1 gm^{-2} , about 20% of the
388 estimated chloride deposition, while in the eastern half, average uncertainty is over 1.5 gm^{-2} ,
389 about 50% of the estimated chloride deposition (Fig. 7d). This value is similar or larger than
390 the cross-validation MAE values. The mapping uncertainty at the sampling sites is small.
391 The mean absolute error of the regression estimates at the 15 sites is 0.54 gm^{-2} , equivalent to
392 14% of the average observed annual chloride deposition at these sites (Table 3) (Fig. 6b).
393 After the residual kriging is added, the mean absolute error over the 17 sites is reduced to
394 0.41 gm^{-2} (Figure 6b, this is different from cross validation results shown in Figure 6a), about
395 11% of the average observed annual deposition at these sites. A long term mean precipitation

396 map was previously constructed for the study area, based on a much denser observation
397 network (96 gauges) and a much longer observation period (the majority of these data have
398 over 30 years record) (Guan et al., 2009). The average uncertainty of the precipitation map is
399 about 2% at 90% confidence level. Based on this, and the chloride deposition maps, a bulk
400 chloride concentration map (Fig. 7e) and its uncertainty map (Fig. 7f) are provided. The
401 uncertainty in the precipitation mapping is neglected when chloride concentration uncertainty
402 is calculated because of the low precipitation mapping uncertainty. The map (Fig. 7e) shows
403 that bulk chloride concentration is about 5 mg/l in the centre of the MLR, increasing
404 westward toward the coast and southeast-ward, to above 10 mg/l. The uncertainty in bulk
405 chloride concentration is 1-1.5 mg/l for the central of the MLR, about 30% of estimated
406 chloride concentration (Fig. 7f). This level of uncertainty is similar to that using much
407 expensive $^{36}\text{Cl}/\text{Cl}$ method (Scanlon, 2000). However, due to the sparse sample points in the
408 eastern part of the study area, the uncertainty is around and above 50% of the estimated
409 chloride concentration. More sampling points are recommended for the future in this portion
410 of the area.

411 4. Discussion

412 It is interesting to observe that elevation does not significantly influence chloride
413 deposition, although it enhances precipitation in the study area. This result implies that This
414 result suggests either that chloride wet deposition does not increase proportionally with
415 precipitation, or that the increase in wet deposition with elevation is compensated by a
416 decrease in dry deposition with elevation, or both. It is well understood that a larger aerosol
417 removal rate occurs during the earlier time of a rainfall event (Goncalves et al., 2002). Thus,
418 chloride concentration in rain water decreases with an increase of rainfall amount. This
419 phenomenon is observed in the Chloride concentration in instantaneous rain samples may
420 give us some hint on how wet deposition is related to precipitation rate collected in the study
421 area. A series of 1.6-mm rain samples were collected over a period with in a single rainfall
422 event (about 30 mm precipitation) on Flinders University campus on May 5th, 2008 (Fig. 8).
423 It is observed that chloride concentration varies in a range between 3 and 17 mg/l. During the
424 seven hour period, chloride concentration peaks at 9:00, 11:30, and 15:40. The subsequent
425 rain samples after the peak times s have lower chloride concentration. This indicates that the
426 peak concentration samples were resulted from raindrops probably condensed-formed earlier
427 in the source cloud which dissolved more chloride-bearing aerosols scavenged more in-cloud
428 and below-cloud chloride aerosols, with the subsequent rain drops having less chloride

429 aerosols to include. If we assume a similar mechanism applies to the whole area, it is easy to
430 understand why wet deposition does not increase proportionally with precipitation. This is
431 supported by the weak partial correlation between chloride deposition (D) and precipitation
432 (P) when coastal distance (X) effect is removed (Fig. 4). Nevertheless, D is positively
433 correlated (although not statistically significant, $r = 0.21$) to elevation (Z) when X effect is
434 removed, suggesting elevation does weakly facilitate wet deposition, by increasing
435 precipitation, but not in the same proportion to its effect on increasing precipitation. ~~When X
436 and P effect is removed, partial correlation between D and Z becomes negative. This result
437 indicates that dry deposition slightly decreases with elevation. As elevation affects both wet
438 and dry deposition in an opposite way, the chloride deposition becomes elevation-
439 independent in the study area.~~

440 Another interesting finding is that chloride deposition in the east-facing slope is
441 significantly larger than the west-facing slope when coastal distance effect is removed.
442 Previously, we thought that the western slope, facing incoming chloride-bearing aerosols flux,
443 might intercept atmospheric chloride and enhance deposition. This hypothesis is not
444 supported by the correlation analysis results. As wind plays an important role in aerosol
445 transport, analysis of wind direction may give us some hint. In Fig. 9, average sine values of
446 wind direction at 09:00 a.m. (~~representing night-time wind~~) and 03:00 p.m. (~~representing
447 daytime wind~~) are plotted against the longitude. Due to land-sea circulation, sea breeze
448 dominates daytime wind climate in the coastal area, and the 03:00 p.m. observation
449 represents the direction of daytime sea breeze direction. The sine value is positive if the wind
450 comes from the east, and negative if the wind comes from the west. During the day time,
451 westerly winds dominate in the study area, which may facilitate aerosol transport to the east.
452 When the westerly air mass is constrained by the topographic barrier on the western slope,
453 windspeed increases, and reaches the maximum at the upwind side of the hill. The windspeed
454 decreases over the downwind slope. This phenomenon has been extensively studied in sand
455 dune formation processes (Andreotti et al., 2002). The elevated wind speed at the upwind
456 slope facilitates atmospheric chloride transport, and a decreased wind speed at the downwind
457 slope facilitates chloride deposition, which may explain the positive partial correlation
458 between D and $\beta \sin \alpha$ from the data. The above discussion is based on that the ocean to the
459 west of the study area is the only source of atmospheric chloride. Without further sampling
460 and examination, other possibility cannot be excluded. For example, the positive partial
461 correlation between D and $\beta \sin \alpha$ may be an artefact from local dust recycling, or local

462 | atmospheric chloride sources. In the eastern flank of MLR, with dry climate, local dust may
463 | have higher chloride content than that in the western flank. If local dust brings some local
464 | chloride to the BCD collectors, it may cause the difference between the two sides, leading to
465 | similar statistical association between D and $\beta \sin \alpha$. If local chloride recycle happens, the
466 | chloride map constructed based on the observation data would slightly overestimate actual
467 | atmospheric BCD in the eastern flank.

468 | 5. Conclusions

469 | Bulk chloride deposition in the Mount Lofty Ranges, a coastal hilly area in South
470 | Australia, was examined with selected geographical (~~easting and northing~~coastal distance),
471 | orographic (elevation, slope and aspect), and atmospheric (precipitation) variables. Both
472 | partial correlation analysis and regression analysis were performed to understand the
473 | controlling factors in annual chloride deposition. The results support that westerly marine
474 | source provides aerosols for BCD in the most part of the study area, and indicate that the
475 | ~~easting value of the site (equivalent to~~ coastal distance ~~);~~ and terrain aspect and slope are two
476 | significant factors controlling chloride deposition. Coastal distance accounts for about 65% of
477 | the spatial variability in chloride deposition, with terrain aspect and slope accounting for
478 | about 8%. The deposition gradient is about $0.08 \text{ gm}^{-2}\text{year}^{-1}\text{km}^{-1}$ inland, within the range
479 | reported for other areas. The correlation results suggest that more chloride deposition occurs
480 | at the eastern slope than the western slope of MLR. Elevation does not significantly influence
481 | chloride deposition in the study area. The results also indicate that elevation slightly enhances
482 | ~~wet deposition via increasing precipitation, but not in proportion to its effect on precipitation.~~
483 | ~~Meanwhile, dry deposition is slightly weaker at higher elevations. These two opposite effects~~
484 | ~~result in apparent elevation independent chloride deposition in the study area.~~

485 | Based on the regression analysis results, a published de-trended residual kriging
486 | mapping procedure (ASOADEK) was applied to construct the annual chloride deposition map
487 | and bulk chloride concentration map. The average uncertainty of the deposition map is about
488 | 20% in the western MLR, comparable to that of the $^{36}\text{Cl}/\text{Cl}$ method, and over 50% in the
489 | eastern MLR where more future sampling is recommended. The maps will be useful to
490 | examine catchment chloride balance for the CMB application in the study area, which will be
491 | the subject of a separate paper.

492

493 Acknowledgment

494 Constructive discussion with Graham Green and Erick Bestland is appreciated. The
495 Department of Water, Land and Biodiversity Conservation of South Australia provided some
496 precipitation chloride data, and GIS layers. Bureau of Meteorology provided long-term
497 precipitation data, and wind speed data. Stacey Priestley (Flinders University), Darren Ray
498 (BOM), Tania Wilson, Graham Green, and Eddie Banks (DWLBC) and Russell Jones (Water
499 Data Services), assisted in data preparation.

500

501 **References:**

- 502 Alcalá, F.J. and Custodio, E.: Atmospheric chloride deposition in continental Spain. *Hydrol.*
503 *Process.*, 22(18), 3636-3650, 2008a.
- 504 Alcalá, F.J. and Custodio, E.: Using the Cl/Br ratio as a tracer to identify the origin of salinity
505 in aquifers in Spain and Portugal. *Journal of Hydrology*, 359(1-2), 189-207, 2008b.
- 506 Andreotti, B., Claudin, P. and Douady, S.: Selection of dune shapes and velocities - Part 1:
507 Dynamics of sand, wind and barchans. *Eur. Phys. J. B*, 28(3), 321-339, 2002.
- 508 Biggs, A.J.W.: Rainfall salt accessions in the Queensland Murray-Darling Basin. *Australian*
509 *Journal of Soil Research*, 44(6), 637-645, 2006.
- 510 Blackburn, G. and McLeod, S.: Salinity of Atmospheric Precipitation in the Murray-Darling
511 Drainage Division, Australia. *Australian Journal of Soil Research*, 21, 411-434, 1983.
- 512 BOM: Bureau of Meteorology of Australia, www.bom.gov.au, visited 2009.
- 513 Carratala, A., Gomez, A. and Bellot, J.: Mapping rain composition in the east of Spain by
514 applying kriging. *Water Air and Soil Pollution*, 104(1-2), 9-27, 1998.
- 515 Contreras, S., Boer, M.M., Alcalá, F.J., Domingo, F., Garcia, M., Pulido-Bosch, A. and
516 Puigdefabregas, J.: An ecohydrological modelling approach for assessing long-term
517 recharge rates in semiarid karstic landscapes. *Journal of Hydrology*, 351(1-2), 42-57,
518 2008.
- 519 Cook, P.G., Edmunds, W.M. and Gaye, C.B.: Estimating paleorecharge and paleoclimate
520 from unsaturated zone profiles. *Water Resour. Res.*, 28(10), 2721-2731, 1992.
- 521 Deutsch, C.V. and Journel, A.G.: *GSLIB--Geostatistical Software Library and User's Guide*.
522 *Applied Geostatistics Series*. Oxford University Press, New York, 369 pp, 1998.
- 523 Dunn, S.M. and Bacon, J.R.: Assessing the value of Cl- and delta O-18 data in modelling the
524 hydrological behaviour of a small upland catchment in northeast Scotland. *Hydrol.*
525 *Res.*, 39(5-6), 337-358, 2008.
- 526 Edmunds, W.M., Fellman, E., Goni, I.B. and Prudhomme, C.: Spatial and temporal
527 distribution of groundwater recharge in northern Nigeria. *Hydrogeol. J.*, 10(1), 205-
528 215, 2002.
- 529 Eriksson, E.: The yearly circulation of chloride and sulphur in nature; meteorological,
530 geochemical and pedological implications, part II. *Tellus*, 11(4), 375-403, 1959.
- 531 Eriksson, E.: The yearly circulation of chloride and sulphur in nature; meteorological,
532 geochemical and pedological implications, part II. *Tellus*, 12, 63-109, 1960.
- 533 Eriksson, E. and Khunakasem, V.: Chloride concentrations in groundwater, recharge rate and
534 rate of deposition of chloride in the Israel coastal plain. *Journal of Hydrology*, 7, 178-
535 197, 1969.
- 536 Friedman, I., Smith, G.I., Gleason, J.D., Warden, A. and Harris, J.M.: Stable isotope
537 composition of waters in southeastern California. 1. Modern precipitation. *J. Geophys.*
538 *Res.-Atmos.*, 97(D5), 5795-5812, 1992.
- 539 [Goncalves, F.L.T., Andrade, M.F., Forti, M.C., Astolfo, R., Ramos, M.A., Massambani, O.](#)
540 [and Melfi, A.J.: Preliminary estimation of the rainfall chemical composition evaluated](#)
541 [through the scavenging modeling for north-eastern Amazonian region \(Amapa State,](#)
542 [Brazil\). *Environ. Pollut.*, 121\(1\), 63-73, 2003.](#)
- 543 Goovaerts, P.: Geostatistical approaches for incorporating elevation into the spatial
544 interpolation of rainfall. *Journal of Hydrology*, 228(1-2), 113-129, 2000.
- 545 Guan, H., Simmons, C.T. and Love, A.J.: Orographic controls on rain water isotope
546 distribution in the Mount Lofty Ranges of South Australia. *Journal of Hydrology*,
547 374(3-4), 255-264, 2009.

- 548 Guan, H., Wilson, J.L. and Makhnin, O.: Geostatistical mapping of mountain precipitation
549 incorporating autosearched effects of terrain and climatic characteristics. *Journal of*
550 *Hydrometeorology*, 6(6), 1018-1031, 2005.
- 551 Gustafsson, M.E.R. and Larsson, E.H.: Spatial and temporal patterns of chloride deposition in
552 Southern Sweden. *Water Air and Soil Pollution*, 124(3-4), 345-369, 2000.
- 553 Hrachowitz, M., Soulsby, C., Tetzlaff, D., Dawson, J.J.C. and Malcolm, I.A.: Regionalization
554 of transit time estimates in montane catchments by integrating landscape controls.
555 *Water Resour. Res.*, 45, 18, 2009.
- 556 Isaaks, E.H. and Srivastava, R.M.: *Applied Geostatistics*. Oxford University Press, Inc, 561
557 pp, 1989.
- 558 Kayaalp, A.S.: Application of rainfall chemistry and isotope data to hydro-meteorological
559 modelling. Ph.D. Thesis, Flinders University, Adelaide, Australia, 273 pp, 2001.
- 560 Keywood, M.D., Chivas, A.R., Fifield, L.K., Cresswell, R.G. and Ayers, G.P.: The accession
561 of chloride to the western half of the Australian continent. *Australian Journal of Soil*
562 *Research*, 35(5), 1177-1189, 1997.
- 563 Kirchner, J.W., Feng, X.H. and Neal, C.: Fractal stream chemistry and its implications for
564 contaminant transport in catchments. *Nature*, 403(6769), 524-527, 2000.
- 565 Lewis, E.R. and Schwartz, S.E.: *Sea Salt Aerosol Production: Mechanisms, Methods,*
566 *Measurements and Models -- A Critical Review*. Geophysical Monograph 152.
567 American Geophysical Union, Washington, DC, 413 pp, 2004.
- 568 Lowry, R.: *Concepts and Applications of Inferential Statistics*.
569 <http://faculty.vassar.edu/lowry/webtext.html>, Vassar College, Poughkeepsie, NY
570 USA, 1999-2009.
- 571 Minor, T.B., Russell, C.E. and Mizell, S.A.: Development of a GIS-based model for
572 extrapolating mesoscale groundwater recharge estimates using integrated geospatial
573 data sets. *Hydrogeol. J.*, 15(1), 183-195, 2007.
- 574 Moreno, G., Gallardo, J.F. and Bussotti: Canopy modification of atmospheric deposition in
575 oligotrophic *Quercus pyrenaica* forests of an unpolluted region (central-western
576 Spain). *For. Ecol. Manage.*, 149(1-3), 47-60, 2001.
- 577 Phillips, F.M.: Environmental tracers for water movement in desert soils of the American
578 southwest. *Soil Sci. Soc. Am. J.*, 58(1), 15-24, 1994.
- 579 Preiss, W.V.: The Adelaide Geosyncline: Late proterozoic stratigraphy, sedimentation,
580 palaeontology and tectonics. *Bulletin / Geological Survey of South Australia*, 53, 439,
581 1987.
- 582 Scanlon, B.R.: Uncertainties in estimating water fluxes and residence times using
583 environmental tracers in an arid unsaturated zone. *Water Resour. Res.*, 36(2), 395-409,
584 2000.
- 585 Scanlon, B.R., Healy, R.W. and Cook, P.G.: Choosing appropriate techniques for quantifying
586 groundwater recharge. *Hydrogeol. J.*, 10(1), 18-39, 2002.
- 587 Shaw, S.B., Harpold, A.A., Taylor, J.C. and Walter, M.T.: Investigating a high resolution,
588 stream chloride time series from the Biscuit Brook catchment, Catskills, NY. *Journal*
589 *of Hydrology*, 348(3-4), 245-256, 2008.
- 590 Walker, G.R., Jolly, I.D. and Cook, P.G.: A new chloride leaching approach to the estimation
591 of diffuse recharge following a change in land use. *Journal of Hydrology*, 128, 49-67,
592 1991.
- 593 Wilson, J.L. and Guan, H.: Mountain-block hydrology and mountain-front recharge. In: J.F.
594 Hogan, F.M. Phillips and B.R. Scanlon (Editors), *Groundwater Recharge in a Desert*
595 *Environment: The Southwestern United States*. Water Science and Applications
596 Series. American Geophysical Union, Washington, D.C., pp. 113-137, 2004.

597 Wood, W.W. and Sanford, W.E.: Chemical and isotopic methods for quantifying
598 groundwater recharge in a regional, semiarid environment. *Ground Water*, 33(3), 458-
599 468, 1995.
600
601

Figure captions:

Figure 1 The DEM map of the study area with 17 sampling sites (crossed circles) of bulk chloride, with insert maps of Australia and South Australia showing the regional location of the study area, and an insert map of annual precipitation overlain by 41 wind observation sites (stars). The numbers next to the chloride sites correspond to those in Table 1. The Bureau of Meteorology IDs of the four selected wind sites from northwest to southeast are 23090 (W1), 23733 (W2), 23842 (W3), and 24545 (W4). The longitude and latitude marks are for the DEM map.

Figure 2 Histograms of wind direction observed at 9:00AM (left column) and 3:00PM (right column) for four selected wind observation sites (W1, W2, W3, and W4 in Figure 1). Horizontal axis shows bin centres of the wind direction in degree clockwise from the north. The data were collected by BOM in 1977-2008, 1957-2008, 1987-2008, and 1965-1969 for the four sites, respectively.

Figure 3 Annual chloride deposition vs. UTM Easting (as a proxy for coastal distance), with sites #16 and #17 excluded). The numbers next to the symbols correspond to those in Table 1 and Figure 1.

Figure 4 (Partial) correlation coefficient between yearly chloride deposition and each of the selected variables, with or without the effects of other variables (specified in the bracket) removed. The dash line is 90% significance for easy comparison between correlations.

Figure 5 Calculated semivariograms with a 10-km lag separation distance, and a 2-km lag tolerance, and the model fitting for (a) one cross validation set of observed annual mean chloride deposition, and (b) regression de-trended residuals over the 17 sites. The fitted model is a Gaussian model (range = 48 km, sill = $1.8 \text{ (gm}^{-2})^2$, and nugget = $0.05 \text{ (gm}^{-2})^2$) for (a), and a spherical model (range = 40 km, sill = $0.29 \text{ (gm}^{-2})^2$, and nugget = $0.2 \text{ (gm}^{-2})^2$) for (b).

Figure 6 (a) Cross-validation estimates of regression, ASOADEK, and direct ordinary kriging, and (b) regression estimates of annual chloride deposition (for the 15 sites) and ASOADEK estimates (for all 17 sites), in comparison to the observations. The MAE values are mean absolute errors (g/m^2) of the observation sites, and the r values are Pearson correlation coefficients between the estimates and the observations.

Figure 7 Various mapping results of annual chloride deposition and related quantities over the study area: (a) regression map, (b) residual kriging map, (c) ASOADEK map, (d) ASOADEK map uncertainty, (e) bulk chloride concentration map, and (f) concentration map uncertainty. The uncertainty is estimated at 90% confidence level. The cross symbols on (d) is the bulk chloride sampling sites (Figure 1). The missing data in the southwest corner on the maps of b through f is because the residual kriging does not produce reasonable estimates due to lack of data over this part of the area.

Figure 8 Chloride concentration in each of the sequential 1.6 mm rain samples collected at Flinders University campus on 16/5/2008.

Figure 9 Mean values of $\sin(\text{wind direction})$ at the 41 observation sites (Figure 1) for two seasons: (a) summer months (12, 1, 2), and (b) winter months (6, 7, 8).

Table 1. Bulk chloride deposition and concentration over the Mount Lofty Ranges calculated from samples collected over two periods by DWLBC (1-8) and Flinders University (9-17), and associated site information

ID	Site id	Site name	Easting (m)	Northing (m)	Elevation ¹ (m)	Aspect (°)	Slope (°)	Precip. ² (mm)	Data period m/y-m/y	Concentration ³ (mg/l)	Deposition (g/m ² /yr)
1	AW503502	Scott Creek	287895	6113235	272	246	0.09	751	02/03-02/05	5.4	4.05
2	AW426638	Mount Barker	306288	6117246	323	121	0.06	705	11/02-11/04	6.1	4.63
3	AW504512	Mt Pleasant	319631	6148870	425	132	0.03	731	12/02-10/03	5.2	2.57
4	AW504559	Cherryville	295316	6134505	531	303	0.15	1000	01/03-07/03	4.2	4.37
5	AW504563	Milbrook	300896	6143374	328	310	0.08	728	07/03-03/04	5.9	3.65
6	AW505517	Penrice	321661	6184765	314	296	0.06	557	12/03-11/04	4.1	1.98
7	AW505537	Mount Adam	318897	6165439	515	50	0.00	868	11/02-11/04	4.1	3.32
8	AW505500	Warren Reservoir	309409	6157186	391	290	0.10	778	10/03-11/04	4.8	3.99
9	Kyp02	Hallett Cove	273701	6115600	125	281	0.13	654	04/92-12/94	12.2	6.97
10	Kyp03	Bedford Park	278584	6121170	161	291	0.17	638	04/92-12/94	6.0	3.97
11	Kyp04	Happy Valley	279315	6115516	149	274	0.15	692	06/92-11/94	4.9	3.78
12	Kyp05	Flagstaff Hill	279991	6118507	180	282	0.17	714	06/92-12/94	6.5	5.10
13	Kyp06	Heathfield	292858	6120585	414	220	0.07	983	07/92-12/94	4.7	4.76
14	Kyp07	Hahndorf	300232	6121471	340	155	0.05	796	07/92-12/94	5.1	4.67
15	Kyp08	Mannum	345887	6135339	47	155	0.02	280	06/92-12/94	3.7	1.33
16	Kyp09	Murray Bridge	342703	6112274	9	104	0.03	340	06/92-12/94	6.1	2.54
17	Kyp10	Tailem Bend	359324	6097715	12	214	0.02	430	07/92-12/94	5.7	2.59

1. The elevation is 1-km pixel elevation, while aspect and slope are 7-km pixel values optimized in the regression.
2. Precipitation is annual precipitation estimated based on long-term observations (Guan et al., 2009).
3. This is weight mean bulk chloride concentration.

Table 2 Correlation matrix of chloride deposition and selected variables for sites #1-15 (P is long-term mean annual precipitation, other symbols are described in Eq. (4), the correlation coefficients in bold face are significant at 90% confidence level).

	<i>D</i>	<i>P</i>	<i>X</i>	<i>Y</i>	<i>Z</i>	$\beta\cos(\alpha)$	$\beta\sin(\alpha)$
D	1						
P	0.48	1					
X	-0.81	-0.41	1				
Y	-0.61	-0.09	0.65	1			
Z	-0.03	0.79	0.19	0.44	1		
$\beta\cos(\alpha)$	0.09	0.05	-0.28	0.22	0.01	1	
$\beta\sin(\alpha)$	-0.41	-0.12	0.74	0.29	0.32	-0.67	1

Table 3 Regression results of chloride deposition with X , X and $\beta \sin \alpha$, respectively, based on observations of sites 1-15 (the 15-site average mean annual chloride deposition is 3.94 g/m²)

Predictor variables		b_0	$b_1 X$	$b_5 \beta \sin \alpha$	R^2	Adjusted ^a R^2	MAE ^b
X	coefficients	9.40	-0.054		0.65	0.62	0.63
	p values	1E-06	3E-04				
$X, \beta \sin \alpha$	coefficients	11.95	-0.075	7.72	0.73	0.68	0.54
	p values	0.0000	0.0003	0.090			

a. Adjusted coefficient of multiple determination considering the number of predictor variables effect.

b. MAE is the regression mean absolute error (g/m²).

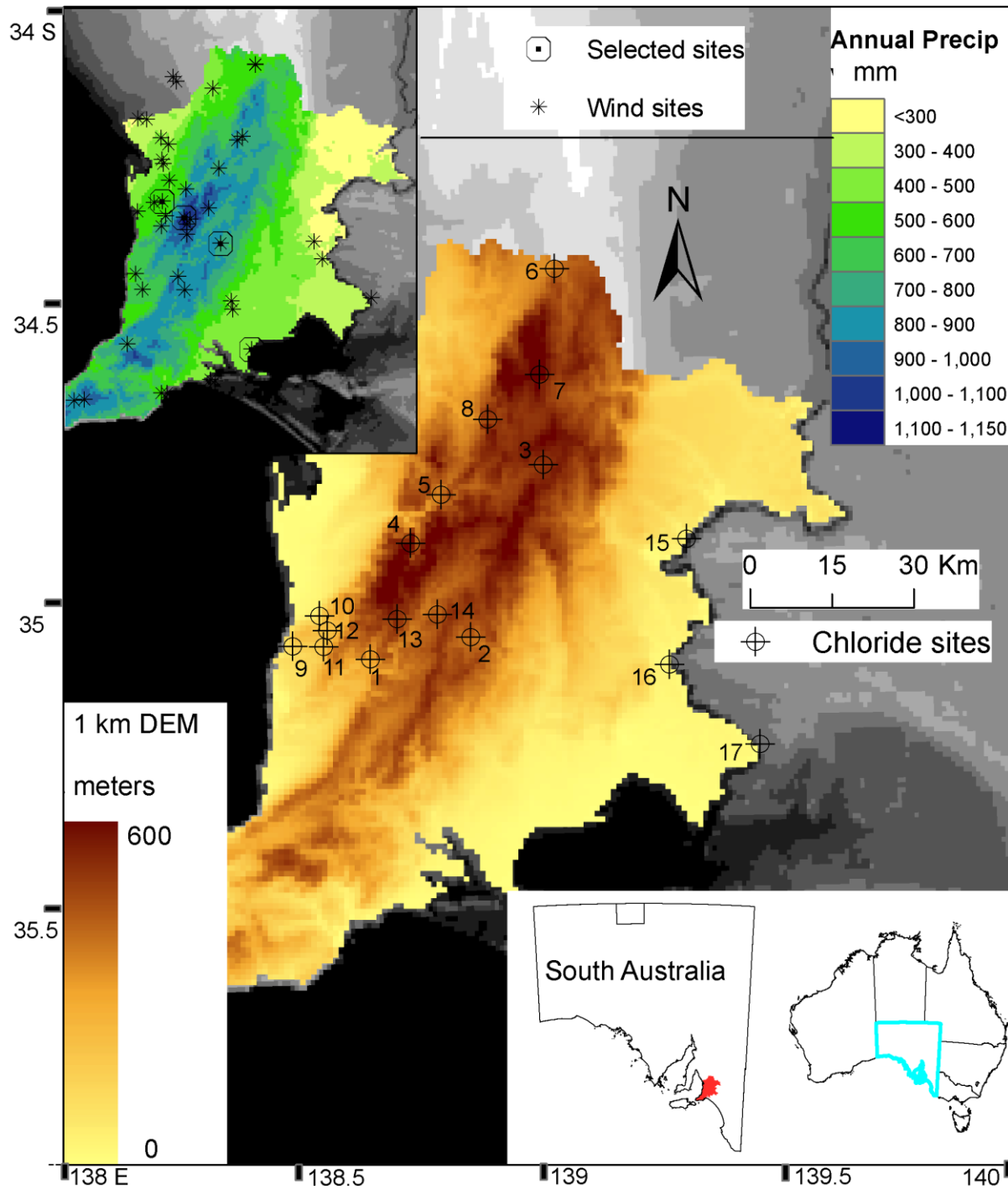


Figure 1 The DEM map of the study area with 17 sampling sites (crossed circles) of bulk chloride, with insert maps of Australia and South Australia showing the regional location of the study area, and an insert map of annual precipitation overlain by 41 wind observation sites (stars). The numbers next to the chloride sites correspond to those in Table 1. The Bureau of Meteorology IDs of the four selected wind sites from northwest to southeast are 23090 (W1), 23733 (W2), 23842 (W3), and 24545 (W4). The longitude and latitude marks are for the DEM map.

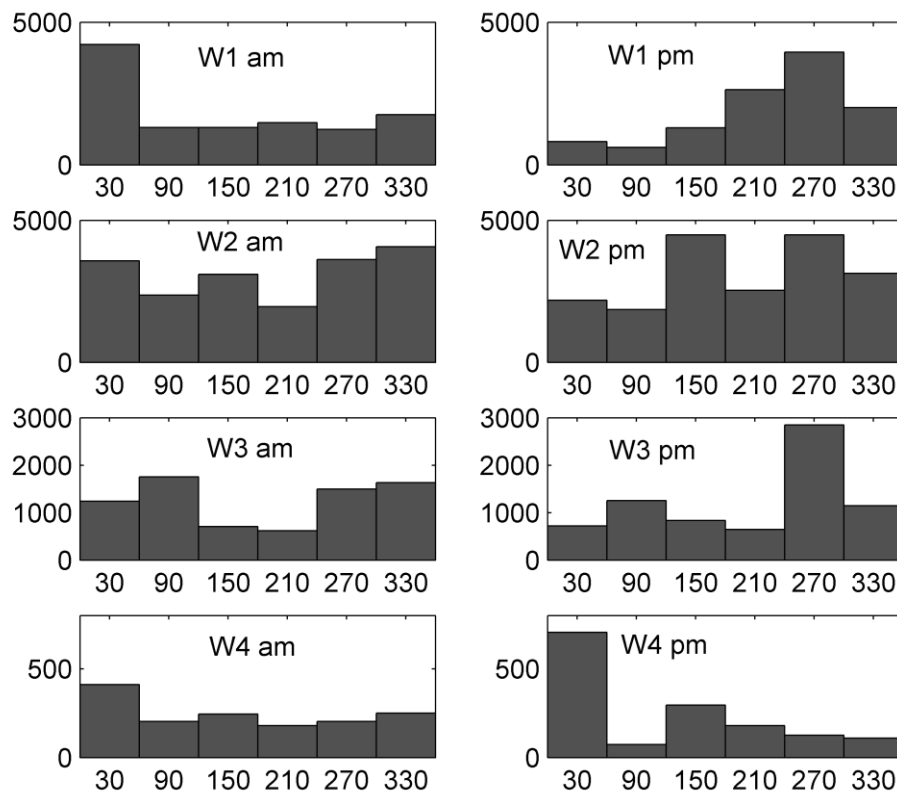


Figure 2 Histograms of wind direction observed at 9:00AM (left column) and 3:00PM (right column) for four selected wind observation sites (W1, W2, W3, and W4 in Figure 1). Horizontal axis shows bin centres of the wind direction in degree clockwise from the north. The data were collected by BOM in 1977-2008, 1957-2008, 1987-2008, and 1965-1969 for the four sites, respectively.

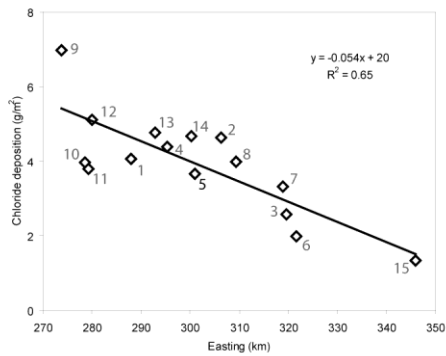


Figure 3 Annual chloride deposition vs. UTM Easting (as a proxy for coastal distance), with sites #16 and #17 excluded). The numbers next to the symbols correspond to those in Table 1 and Figure 1.

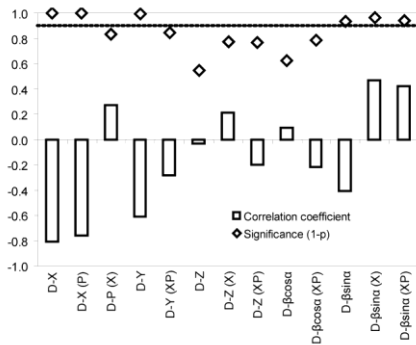


Figure 4 (Partial) correlation coefficient between yearly chloride deposition and each of the selected variables, with or without the effects of other variables (specified in the bracket) removed. The dash line is 90% significance for easy comparison between correlations.

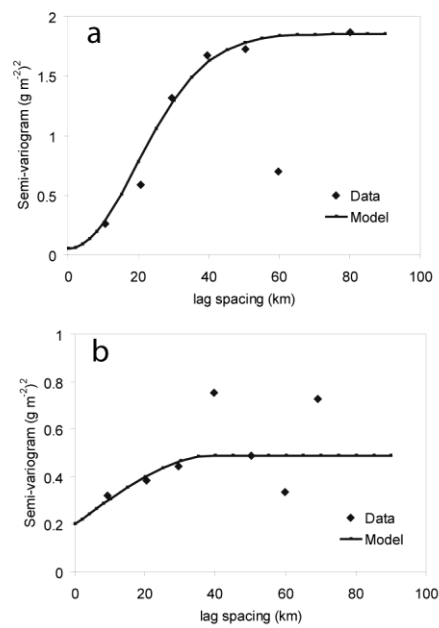


Figure 5 Calculated semivariograms with a 10-km lag separation distance, and a 2-km lag tolerance, and the model fitting for (a) one cross validation set of observed annual mean chloride deposition, and (b) regression de-trended residuals over the 17 sites. The fitted model is a Gaussian model (range = 48 km, sill = $1.8 \text{ (gm}^{-2}\text{)}^2$, and nugget = $0.05 \text{ (gm}^{-2}\text{)}^2$) for (a), and a spherical model (range = 40 km, sill = $0.29 \text{ (gm}^{-2}\text{)}^2$, and nugget = $0.2 \text{ (gm}^{-2}\text{)}^2$) for (b).

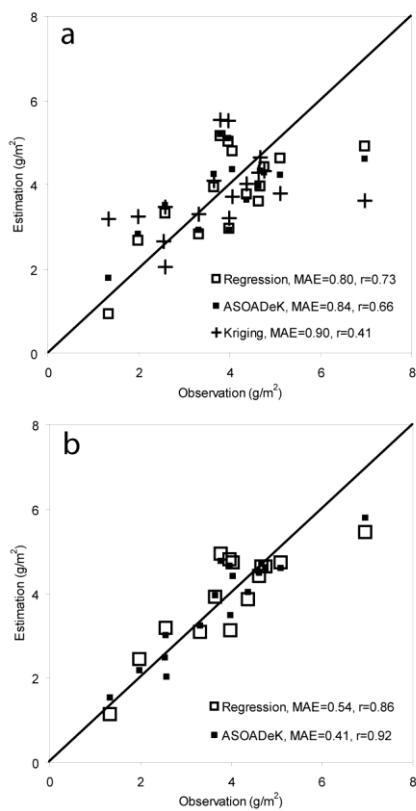


Figure 6 (a) Cross-validation estimates of regression, ASOADEK, and direct ordinary kriging, and (b) regression estimates of annual chloride deposition (for the 15 sites) and ASOADEK estimates (for all 17 sites), in comparison to the observations. The MAE values are mean absolute errors (g/m^2) of the observation sites, and the r values are Pearson correlation coefficients between the estimates and the observations.

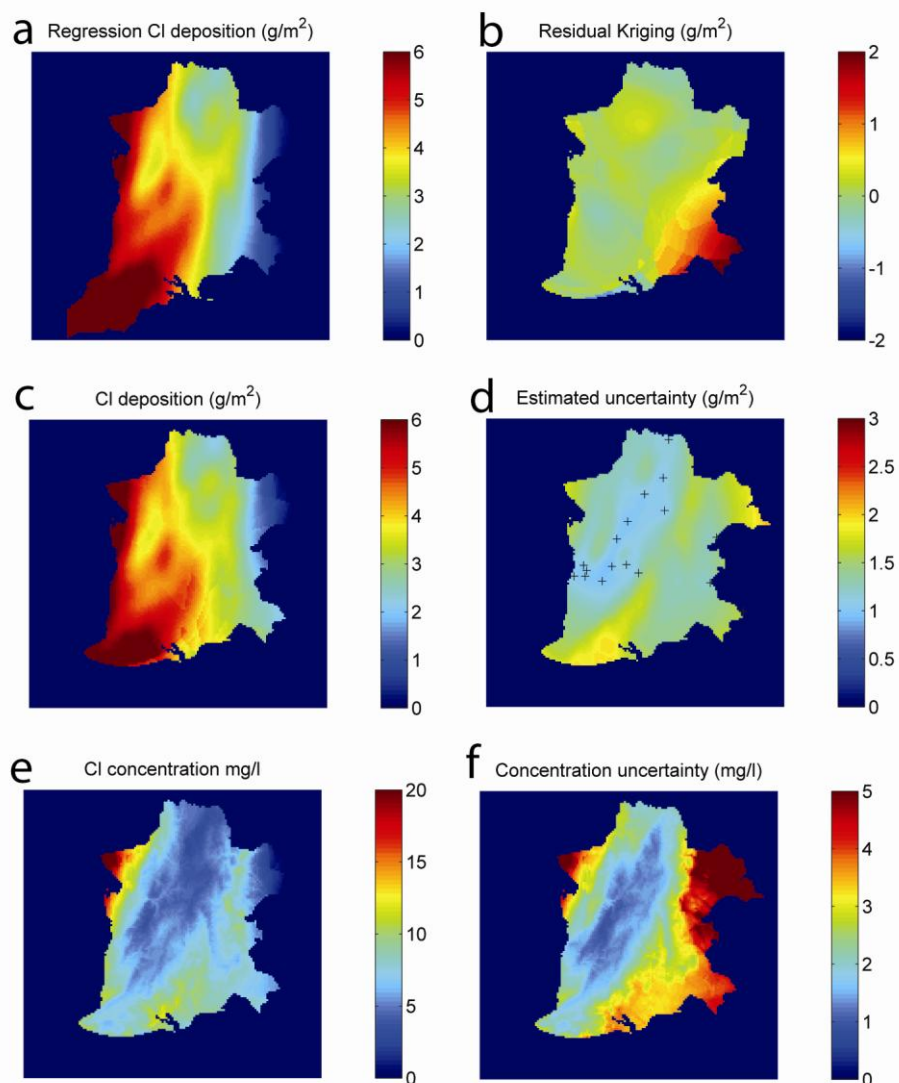


Figure 7 Various mapping results of annual chloride deposition and related quantities over the study area: (a) regression map, (b) residual kriging map, (c) ASODeK map, (d) ASODeK map uncertainty, (e) bulk chloride concentration map, and (f) concentration map uncertainty. The uncertainty is estimated at 90% confidence level. The cross symbols on (d) is the bulk chloride sampling sites (Figure 1). The missing data in the southwest corner on the maps of b through f is because the residual kriging does not produce reasonable estimates due to lack of data over this part of the area.

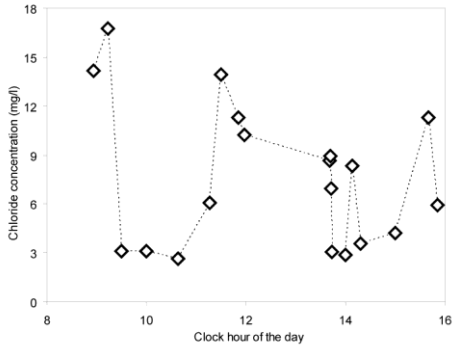


Figure 8 Chloride concentration in each of the sequential 1.6 mm rain samples collected at Flinders University campus on 16/5/2008.

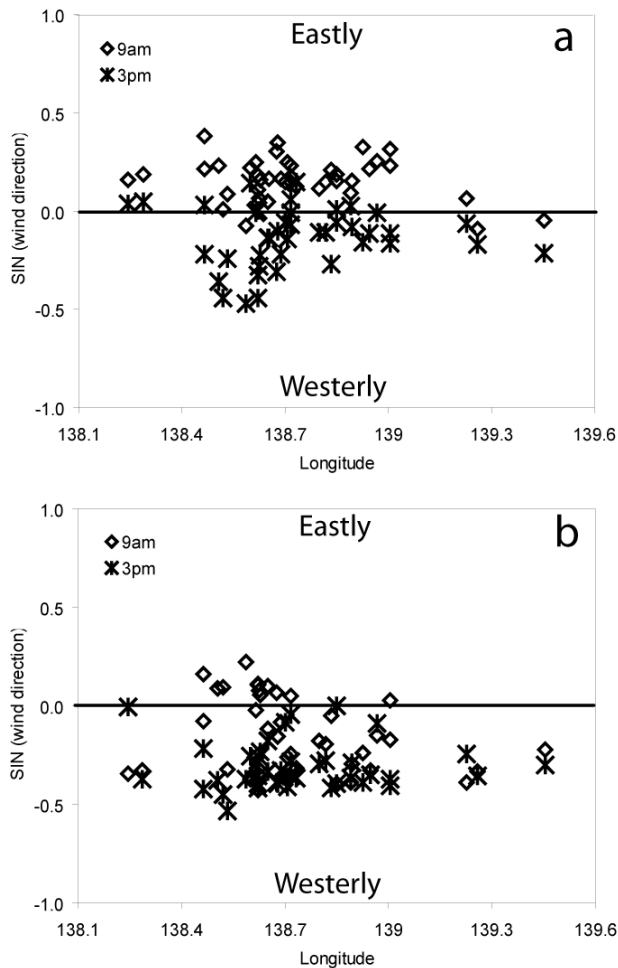


Figure 9 Mean values of $\sin(\text{wind direction})$ at the 41 observation sites (Figure 1) for two seasons: (a) summer months (12, 1, 2), and (b) winter months (6, 7, 8).